Phosphate Binding in the Active Site of Alkaline Phosphatase and the Interactions of 2-Nitrosoacetophenone with Alkaline Phosphatase-Induced Small Structural Changes

Le Zhang, René Buchet, and Gérard Azzar
Université Claude Bernard Lyon I, UFR Chimie-Biochimie UMR CNRS 5013, 69622 Villeurbanne Cedex, France

ABSTRACT To monitor structural changes during the binding of P*i* to the active site of mammalian alkaline phosphatase in water medium, reaction-induced infrared spectroscopy was used. The interaction of P*i* with alkaline phosphatase was triggered by a photorelease of ATP from the inactive P^3-[1-(2-nitrophenyl)]ethyl ester of ATP. After photorelease, ATP was sequentially hydrolyzed by alkaline phosphatase giving rise to adenosine and three P*i*. Although a phosphodiesterase activity was detected prior the photorelease of ATP, it was possible to monitor the structural effects induced by P*i* binding to alkaline phosphatase. Interactions of P*i* with alkaline phosphatase were evidenced by weak infrared changes around 1631 and at 1639 cm^{-1}, suggesting a small distortion of peptide carbonyl backbone. This result indicates that the motion required for the formation of the enzyme-phosphate complex is minimal on the part of alkaline phosphatase, consistent with alkaline phosphatase being an almost perfect enzyme. Photoproduct 2-nitrosoacetophenone may bind to alkaline phosphatase in a site other than the active site of bovine intestinal alkaline phosphatase and than the uncompetitive binding site of L-Phe in bovine intestinal alkaline phosphatase, affecting one-two amino acid residues.

INTRODUCTION

Alkaline phosphatases (AP, EC 3. 1. 3. 1.) are homodimeric metalloenzymes common in both eukaryotes and prokaryotes (Fernley, 1971; Reid and Wilson, 1971). Sequence comparisons between different AP indicated about 25–30% homology between mammalian AP and *Escherichia coli* AP (Bradshaw et al., 1981; Kam et al., 1985; Chang et al., 1986; Weiss et al., 1986; Berger et al., 1987; Henthorn et al., 1988; Millán, 1988; Kim and Wyckoff, 1990; Weissig et al., 1993). Four structural genes encoding human AP have been cloned (Kam et al., 1985; Millán, 1986; Henthorn et al., 1987; Millán and Manes, 1988) corresponding to three tissue-specific AP genes located in chromosome 2 (germ-cell, placenta, and intestinal) and one tissue-nonspecific AP gene located in chromosome 1 (Moss, 1992). The mammalian AP, in contrast to the *E. coli* AP, is a membrane-anchored protein and contains a glycosylphosphatidylinositol anchor linked to the C-terminal carboxyl group of the protein (Low and Finean, 1977; Redman et al., 1994; Ferguson, 1999). Despite differences in their sequences and structures, *E. coli* AP and mammalian AP catalyze the hydrolysis of almost any phosphomonoester with release of inorganic phosphate and alcohol (Fernley, 1971; Reid and Wilson, 1971). Residues involved in the coordination of two Zn^{2+} and one Mg^{2+} ions in the active site and the catalytic serine are preserved from *E. coli* AP (Kim and Wyckoff, 1990) to human placenta AP (Le Du et al., 2001), whereas most of the surrounding residues are different. This suggests that the mechanisms of catalytic reactions are similar for both enzymes, although mammalian AP are inhibited uncompetitively by L-Phe or L-Arg, whereas *E. coli* AP are not (Fishman and Sie, 1970,1971; Lin et al., 1971; Byers et al., 1972; Hummer and Millán, 1991; Hoylaerts et al., 1992). During the hydrolysis of phosphate ester by AP, a serine group of AP is phosphorylated. The transient phosphoenzyme is subsequently hydrolyzed to give a noncovalent enzyme-phosphate complex. Under acidic conditions (pH $<$ 6), the hydrolysis of the phosphoenzyme (k_3, Scheme 1, taken from Holtz and Kantrowitz, 1999) is rate limiting, whereas dissociation of the noncovalent complex of enzyme with bound phosphate is rate limiting at pH $\geq$ 8 (k_4, Scheme 1) (Chlebowski and Coleman, 1972; Hull et al., 1976; Chlebowski et al., 1977; Gettins and Coleman, 1983). The phosphoenzyme may react with alcohol to form a phosphate ester which dissociates from the enzyme (k_5 and k_6, Scheme 1).

Crystal structure, computer modeling and site-directed mutagenesis on human placental AP revealed that amino acids strictly necessary to perform the catalysis are preserved with respect to *E. coli*, whereas a hydrophobic pocket in the vicinity of an active site may account for the specific uncompetitive inhibition of placental AP (Le Du et al., 2001; Kozlenkov et al., 2002; Le Du and Millán, 2002). In addition, x-ray observations confirmed the importance of Asp and Glu residues in the catalytic activity of mammalian placental AP. Asp-91 (numbering for the human placental AP), in the vicinity of catalytic Ser-92, is in a hydrogen-bonding distance of Asn-84 (Le Du et al., 2001). Asn-84, Tyr-367, and Glu-429 are probably involved in the allostery

Submitted September 2, 2003, and accepted for publication February 23, 2004.

Address reprint requests to René Buchet, Université Claude Bernard Lyon I, UFR Chimie-Biochimie UMR CNRS 5013, 6 Rue Victor Grignard, 69622 Villeurbanne Cedex, France. Tel.: 33-4-72-43-13-20; Fax: 33-4-72-43-15-43; E-mail: rbuchet@univ-lyon1.fr.

0006-3495/04/06/3873/09 $2.00

doi: 10.1529/biophysj.103.034116

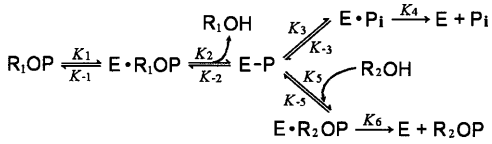

SCHEME 1

(Hoylaerts et al., 1997; Manes et al., 1998; Le Du et al., 2001; Kozlenkov et al., 2002). To probe the mechanisms of hydrolysis by AP, the interaction between vanadate and *E. coli* AP has been determined by x-ray crystallography (Holtz et al., 1999). Unlike the phosphate ion, vanadate forms five-coordinate complex, mimicking a transition state analog. Comparison between *E. coli* AP-vanadate complex and the noncovalent *E. coli* AP-P*i* complex indicates that active site residues moved only slightly (Holtz et al., 1999). The x-ray structure of mammalian placental AP (Le Du et al., 2001), shows that the amino acid residues in the active site are preserved as compared with the x-ray structure of *E. coli* AP. The conformational changes of mammalian AP induced by P*i* binding in water medium were not reported. Based on the similarity of the active site in *E. coli* AP and mammalian AP, one would expect that P*i* binding in mammalian AP would induce similar conformational effects than in *E. coli* AP. Due to the electrostatic interactions between phosphate groups and charged side chain residues, water molecules may play a role in mediating such interactions.

In this work, we investigated the structural changes of mammalian AP in water medium caused by ligand binding in the active site, by using reaction-induced infrared difference spectroscopy (RIDS). RIDS cannot provide a detailed structure of the whole protein as x-ray data do. However, RIDS allows us to measure very small deviations at a single vibrational group, caused by the effects of substrate bindings in the active site of enzymes in water medium (Mäntele, 1993; Siebert, 1995; Cepus et al., 1998; Zscherp and Barth, 2001; Barth and Zscherp, 2002). By taking advantage of the knowledge of the resolved 3D structure of the whole mammalian AP and by measuring small fluctuations of structure changes, we can provide specific details on the deviation of structural changes, such as the magnitude of structural changes (approximate number of amino acids implicated in the ligand binding) as well the changes in hydrogen bond strengths affecting peptide backbone and side chain residues.

EXPERIMENTAL PROCEDURES

Materials

Bovine intestinal alkaline phosphatase (IAP) was a product of Sigma (St. Quentin Fallavier, France). The salts were removed by washing IAP in ^2H_2O buffer (or H_2O buffer for the nondeuterated samples) containing 100 mM Tris-HCl, $p^2H = 7.0$ (or pH 7.4, respectively), 10 mM $MgCl_2$, filtered through millipores (MW, cutoff 30,000). Its purity was checked by gel-electrophoresis. Tris-HCl, Adenosine, were purchased from Roche (Meylan, France). The photolabile ''NPE-caged ATP'', P^3-[1-(2-nitrophenyl)]ethyl ester of ATP was obtained from Molecular Probes Europe (Leiden, the Netherlands).

Infrared spectra of samples in ^2H_2O buffer

Purified IAP (10 mg/ml corresponding to 0.09 mM assuming a 114-KDa dimeric enzyme) were dissolved either in buffer A or in buffer B. ^2H_2O buffer A contained 100 mM Tris-HCl, $p^2H = 7.0$, 10 mM $MgCl_2$ and 2.5–10 mM NPE-caged ATP with or without 5 mM adenosine. ^2H_2O buffer B contained 100 mM phosphate, $p^2H = 7.0$, 10 mM $MgCl_2$ and 4–8 mM NPE-caged ATP with or without 5 mM adenosine. Control samples without protein were prepared under the same conditions. The p^2H was measured with a glass electrode and was corrected by a value of 0.4 (p^2H 7.0 = pH 7.4, Glasoe and Long, 1960). Freshly prepared samples were loaded between two circular CaF_2 windows separated by a 50 μm thick Teflon spacer. They were incubated for 10 min in the dark, before infrared measurements. The infrared cell was thermostated at 20°C with a circulating bath. The optical resolution was 4 cm^{-1} but spectral points were encoded every 2 cm^{-1}. Collected were 256 scans during about 4 min, coadded and Fourier transformed. Then the sample was illuminated for 120 s by means of a 150 W xenon lamp (without filter) to induce complete photorelease of substrates from their cage. The reaction-induced infrared difference spectra (RIDS) of the sample were obtained by subtracting the spectrum measured before illumination from the spectrum measured after the illumination. Five sets of RIDS corresponding to samples in buffer A, whereas three sets of RIDS corresponding to samples in buffer B were measured and coadded to obtain a better signal/noise ratio. The final RIDS were corrected for water-vapor absorption according to Goormaghtigh et al., 1994.

Infrared spectra of samples in H_2O buffer

Purified IAP (50 mg/ml corresponding to 0.45 mM assuming a 114-KDa dimeric enzyme) was prepared in H_2O buffer, containing 200 mM Tris-HCl, pH = 7.4, 10 mM $MgCl_2$ and 20 mM NPE-caged ATP. The same buffer without IAP was used as a control. Freshly prepared samples were loaded between two circular CaF_2 windows separated by a 6 μm thick Teflon spacer. The RIDS were determined under the same conditions as described above. Three sets of RIDS were measured and coadded to obtain a better signal/noise ratio.

RESULTS

Reaction infrared difference spectra of IAP induced by the photorelease of ATP in ^2H_2O Tris-HCl buffer

NPE-caged ATP, protected by a photolabile (2-nitrophenyl)-ethyl group, should not be hydrolyzed by IAP. The 120s illumination induced photolysis of NPE-caged ATP by forming ATP and a 2-nitrosoacetophenone. Since IAP, a proficient phosphomonoesterase, catalyzes a terminal phosphoryl group (Fernley, 1971), the released ATP is hydrolyzed mostly by a stepwise production of three P*i* by forming sequentially ADP, AMP, and adenosine (Fig. 1). However, NPE-caged ATP can be hydrolyzed before the photolysis due to the very low activity of phosphodiesterase of IAP (O'Brien and Herschlag, 2001), especially in the case of relatively high concentration of IAP.

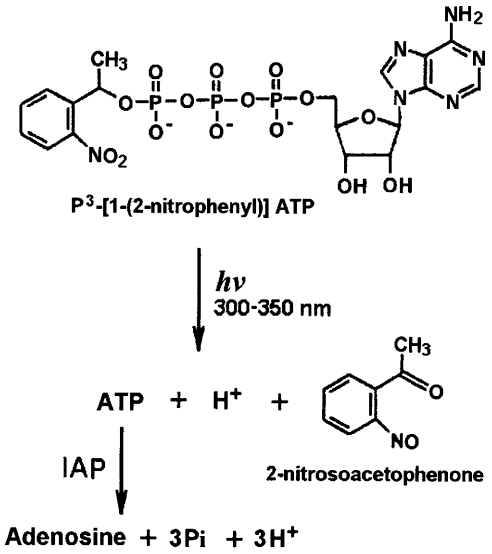

FIGURE 1 Reaction scheme for the photolysis of caged ATP and the hydrolysis of ATP by intestinal alkaline phosphatase.

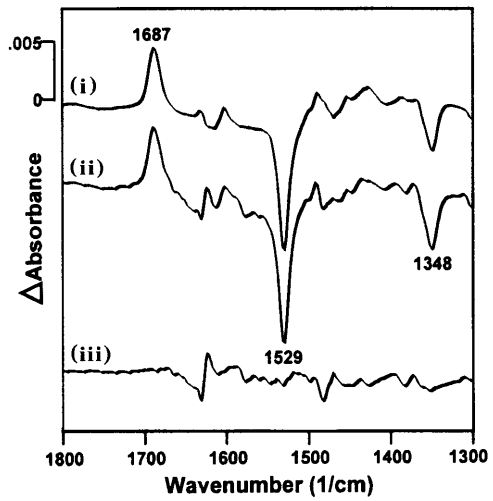

FIGURE 2 Reaction-induced infrared difference spectra of intestinal alkaline phosphatase induced by the photorelease of ATP in ^2H_2O. Reaction-induced infrared difference spectra in the 1800–1300 cm^{-1} region. (*Trace i*) RIDS of caged ATP without AP. (*Trace ii*) RIDS of caged ATP with IAP. (*Trace iii*) Corrected RIDS of caged ATP with IAP corresponding to the difference: spectrum *ii* minus spectrum *i*. The corrected RIDS reflected structural changes caused by binding to IAP after photorelease of ATP from its cage and sequential ATP hydrolysis by IAP. Buffer composition was 100 mM Tris-HCl, $p^2H = 7.0$, 10 mM $MgCl_2$, and 5 mM caged ATP with or without 10 mg/ml (0.09 mM) IAP.

The RIDS, measured before and after photolysis of NPE-caged ATP and complete hydrolysis of ATP by low concentration of IAP, should indicate structural changes caused by the interactions of IAP with adenosine, three P*i*, and photoproduct, 2-nitrosoacetophenone. To determine their respective contributions to the RIDS of NPE-caged ATP and IAP, several control experiments were performed. Tris(hydroxymethyl)aminomethane was used as a buffer since it is a good phosphate acceptor, favoring the formation of a Tris-phosphate complex and its dissociation (k_5 and k_6, Scheme 1) bypassing the dissociation of inorganic phosphate from the enzyme (k_3, Scheme 1) (Trentham and Gutfreund, 1968). The pH of the solution was set at 7.4, which has the advantage to slow down the activity of IAP by a factor of about 35 times as compared with the pH set at 10.5 (Sarrouilhe et al., 1993), whereas the secondary structure of IAP is preserved over the pH range from 7.4 to 10.5 (de La Fournière et al., 1995). The overall infrared spectrum of IAP in the amide-I and amide-II regions was identical to that of IAP previously reported (de La Fournière et al., 1995; Bortolato et al., 1999). UV illumination of IAP without NPE-caged ATP did not produce any infrared changes (results not shown), thus indicating that UV illumination did not affect the secondary structure of IAP. Photoconversion of NPE-caged ATP without protein in Tris-HCl buffer (*trace i* of Fig. 2), induced in the infrared spectrum, two negative bands located at 1527–1530 cm^{-1} and at 1346–1348 cm^{-1} (signaling the disappearance of the nitro group) and a positive band located at 1688–1684 cm^{-1} (indicating the formation of a carbonyl group) (Barth et al., 1990, 1997). The RIDS of NPE-caged ATP with IAP in Tris-HCl buffer (*trace ii* of Fig. 2) is dominated by the photo conversion of NPE-caged ATP. However, small but reproducible changes were observed in the difference spectra (*trace iii* of Fig. 2), corresponding to spectrum *ii* minus spectrum *i*. The 1685–1688 cm^{-1}, 1527–1530 cm^{-1}, and 1346–1348 cm^{-1} bands associated to the photo conversion of NPE-caged ATP were used to normalize the contributions from the photolytic release of the NPE-caged nucleotide between samples (Barth et al., 1991; Cepus et al., 1998; Butler et al., 2002). The difference infrared spectra should reflect structural changes caused by binding of P*i*, adenosine, or 2-nitrosoacetophenone, since infrared spectra were measured before and 5 min after photolysis to ensure complete hydrolysis of ATP by IAP. The structural alterations observed in the 1800–1300 cm^{-1} region (*trace iii* of Fig. 2) were accompanied by changes in phosphate vibrations (Fig. 3). As reported (Barth et al., 1990, 1997; Cepus et al., 1998), the photolysis of NPE-caged GTP or NPE-caged ATP in the absence of protein induced a positive band at 1124–1120 cm^{-1} as well as two negative bands at 1078 cm^{-1} and 1060 cm^{-1} (*trace i* of Fig. 3) indicative of the release of nucleotide from its cage. Photolysis of NPE-caged ATP in the presence of IAP (*trace ii* of Fig. 3) induced changes of phosphate groups caused by the catalytic activity of IAP, indicating complete hydrolysis of ATP. There was no time dependence of the infrared changes after 2 min photolysis and after 5 min collecting the infrared spectra. The magnitude of structural changes of IAP was assessed by determining the ratio of intensities of amide-1 band of IAP in the presence of NPE-caged ATP before photolysis (*spectrum i* in Fig. 4) and its corresponding amide-I change in the RIDS

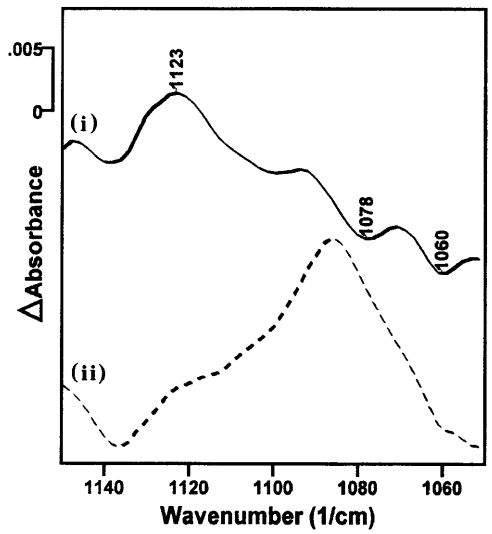

FIGURE 3 Reaction-induced infrared difference spectra of intestinal alkaline phosphatase produced by the photorelease of ATP in ^2H_2O. Reaction infrared difference spectra in the phosphate region. (*Trace i*) RIDS of caged ATP without IAP. (*Trace ii*) RIDS of caged ATP with IAP. Buffer composition was 100 mM Tris-HCl, $p^2H = 7.0$, 10 mM $MgCl_2$ and 5 mM caged ATP with or without 10 mg/ml (0.09 mM) IAP.

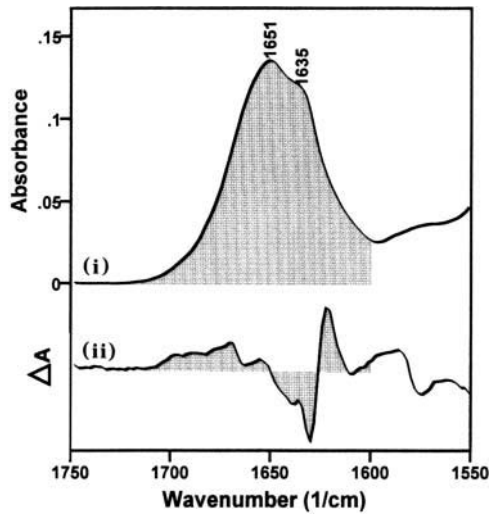

FIGURE 4 Determination of magnitude of structural changes of intestinal alkaline phosphatase caused by the photorelease of ATP in ^2H_2O and its hydrolysis. Trace *i* is the infrared spectrum of caged ATP with IAP before photolysis. Trace *ii* is the corrected RIDS of caged ATP with IAP. Its absorbance scale was expanded 20 times comparatively to the scale for the upper spectrum. For both traces, the buffer composition was 100 mM Tris-HCl, $p^2H = 7.0$, 10 mM $MgCl_2$, and 5 mM NPE-caged ATP with 10 mg/ml (0.09 mM) IAP. The calculated intensity of IR spectrum (*trace i*), corresponding to *A*, and the calculated intensity of RIDS *(trace ii)* corresponding to ΔA, are indicated by shaded surface. The $\Delta A/2A$ ratio, in the 1760–1600 cm^{-1} region, permitted the determination of the magnitude of peptide backbone structural change of IAP induced by the photorelease of ATP and its hydrolysis.

of IAP in the presence of NPE-caged ATP (*spectrum ii* in Fig. 4). The COBSI index (Barth et al., 1996), which is the ratio of intensities $\Delta A/2A$, was 0.0085. This value corresponded to 2 amino acids per monomeric IAP, involved in the structural changes of IAP caused by the binding of P*i*, adenosine, or photoproduct.

Reaction infrared difference spectra of IAP induced by the photorelease of ATP in H_2O Tris-HCl buffer

The same experiment, as described above, was performed in H_2O Tris-HCl buffer instead of ^2H_2O Tris-HCl buffer. To compensate for the low absorbance due to the small pathlength of the infrared cell (6 μm instead of 50 μm), the IAP concentration was increased from 0.09 mM (10 mg/ml) to 0.45 mM (50 mg/ml). The RIDS of NPE-caged ATP in Tris-HCl buffer pH 7.4 (*trace i* of Fig. 5) indicated the three characteristic 1685–1688 cm^{-1}, 1527–1530 cm^{-1}, and 1346–1348 cm^{-1} bands associated to the photoconversion of the NPE-caged ATP, as well as the phosphate bands related to ATP spread over the 950–1150 cm^{-1} region. The RIDS of IAP in the presence of NPE-caged ATP in H_2O Tris-HCl buffer pH 7.4 (*trace ii* of Fig. 5), indicated that the phosphate bands around 950–1150 cm^{-1} disappeared. In contrast, new bands appeared in the phosphate region around 950–1150 cm^{-1} in the RIDS of IAP with NPE-caged ATP in ^2H_2O Tris-HCl buffer p^2H 7.0 (*trace ii* of Fig. 3). These results would suggest that IAP hydrolyzed NPE-caged ATP in H_2O Tris-HCl buffer pH 7.4, before its photorelease, due to its phosphodiesterase activity, which became not negligible at relatively high IAP concentration (0.45 mM). Small changes in the amide-I region were observed in the difference spectra (*trace iii* of Fig. 5), corresponding to spectrum *ii* minus spectrum *i*. The small differences were better evidenced in trace *i* of Fig. 6 and were compared with RIDS of IAP with NPE-caged ATP in ^2H_2O Tris-HCl buffer (*trace ii* of Fig. 6). Both RIDS were different in band shape and magnitude. The negative 1631 cm^{-1} and the 1622 cm^{-1} positive amide-I band with the positive 1586 cm^{-1} and the negative 1577 cm^{-1} side-chain bands observed in the RIDS of IAP in ^2H_2O Tris-HCl buffer (*trace ii* of Fig. 6) disappeared almost completely in the RIDS of IAP in H_2O Tris-HCl buffer (*trace i* of Fig. 6).

Origin of structural changes of IAP after photolysis of NPE-caged ATP

Since the structural changes of IAP were relatively small, the reproducibility of structural changes of IAP was assessed over concentrations of NPE-caged ATP ranging from 2.5 mM to 10 mM. Relatively high amount of NPE-caged ATP and small amount of IAP (down to 0.09 mM) permitted us to increase the fraction of nonhydrolyzed NPE-caged ATP, since the phosphodiesterase activity of IAP cannot be

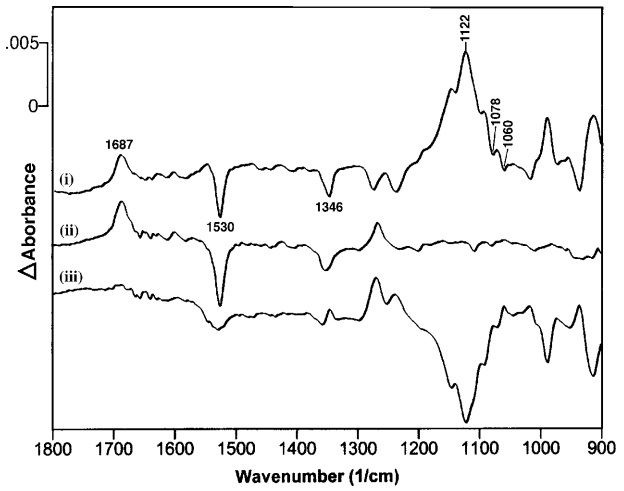

FIGURE 5 Reaction-induced infrared difference spectra of intestinal alkaline phosphatase induced by the photorelease of ATP in H_2O. Reaction-induced infrared difference spectra in the 1800–900 cm^{-1} region. Trace *i* is the RIDS of NPE-caged ATP without IAP; trace *ii* is the RIDS of NPE-caged ATP with IAP; trace *iii* is the corrected RIDS of NPE-caged ATP with IAP corresponding to the difference: spectrum *ii* minus spectrum *i*. Buffer composition was 200 mM Tris-HCl, pH = 7.4, 10 mM $MgCl_2$, and 20 mM NPE-caged ATP with or without 50 mg/ml (0.45 mM) IAP.

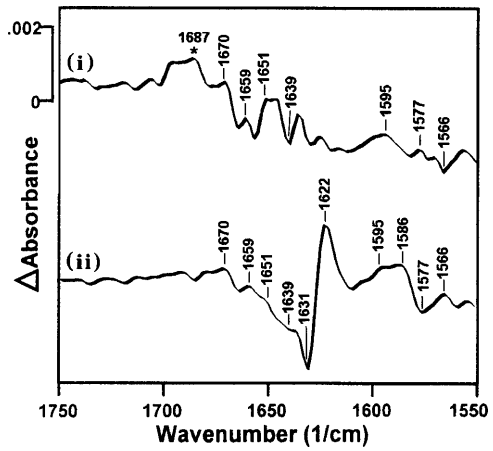

FIGURE 6 Comparison of reaction-induced infrared difference spectra of intestinal alkaline phosphatase produced by the photorelease of ATP from NPE-caged ATP in H_2O and in ^2H_2O buffers. (*Trace i*) Corrected RIDS of NPE-caged ATP with IAP in H_2O buffer. Buffer composition was 200 mM Tris-HCl, pH = 7.4, 10 mM $MgCl_2$, and 20 mM NPE-caged ATP with 50 mg/ml (0.45 mM) IAP. The residual 1687 cm^{-1} peak (indicated by a *star*) corresponds probably to the carbonyl group of the photoproduct, 2-nitrosoacetophenone. (*Trace ii*) Corrected RIDS of NPE-caged ATP with IAP in ^2H_2O buffer. Buffer composition was 100 mM Tris-HCl, $p^2H = 7.0$, 10 mM $MgCl_2$, and 5 mM NPE-caged ATP with 10 mg/ml (0.09 mM) IAP. The absorbance scales of the spectrum *i* has been expanded two times comparatively to the scale for the spectrum *ii*.

neglected. The successive traces (from bottom to top) in Fig. 7 corresponded to the RIDS of IAP in ^2H_2O Tris-HCl buffer with increasing NPE-caged ATP concentrations. Each RIDS of IAP with NPE-caged ATP was corrected for the induced absorption caused by the photolysis of NPE-caged ATP alone. All the RIDS indicated four positive peaks located at 1671 cm^{-1}, 1659–1655 cm^{-1}, 1622 cm^{-1}, and 1585 cm^{-1}, as well as three negative peaks at 1639 cm^{-1}, 1631 cm^{-1}, and at 1576 cm^{-1}. The structural changes observed in the 1700–1600 cm^{-1} region corresponded mostly to structural alterations of the peptide backbone of IAP. The 1585 cm^{-1} and 1576 cm^{-1} bands may correspond either to side-chain vibrations of arginine, or to carboxylate groups of Asp or Glu residues (Chirgadze et al., 1975; Venyaminov and Kalnin, 1990; Goormaghtigh et al., 1994a,b; Barth, 2000). The intensities of the 1639 cm^{-1}, 1631 cm^{-1}, and 1576 cm^{-1} negative peaks, as well as the 1622 cm^{-1} and 1585 cm^{-1} positive peaks, increased by two- to threefold with increasing concentrations of NPE-caged ATP from 2.5 mM to 10 mM (Fig. 7). The increase of the initial NPE-caged ATP concentration and the low IAP concentration could contribute both to the increase of nonhydrolyzed NPE-caged ATP, before the photolysis. Under these conditions the phosphomonoesterase activity can be monitored. Furthermore, the inorganic phosphate is a competitive inhibitor of IAP with Ki = 1.86 ± 0.1 mM (determined in this work under the same conditions as for IR samples), inferring that the structural changes could not have been solely promoted by the interactions of P*i* with IAP. Indeed, a partial saturation of P*i* binding would have been observed, since after complete ATP hydrolysis, three inorganic phosphates were released from 2.5–10 mM NPE-caged ATP, leading to 80–94% saturation of P*i* binding site of IAP.

These findings suggest that, in addition to inorganic phosphate, other products such as adenosine or 2-nitrosoacetophenone may interact with IAP. To determine the contributions of each of them, several controls were performed.

First, a 100 mM phosphate buffer p^2H 7.0 was used instead of 100 mM Tris-HCl buffer p^2H 7.0, to saturate the P*i* binding site of IAP. The RIDS of NPE-caged ATP with IAP in 100 mM Tris-HCl buffer p^2H 7.0 and 10 mM Mg^{2+} (Fig. 8 *A*) was slightly different from that of NPE-caged ATP with IAP in 100 mM phosphate buffer p^2H 7.0 and 10 mM Mg^{2+} (Fig. 8 *B*). Four positive peaks located at 1671 cm^{-1}, 1655–1658 cm^{-1}, 1622–1623 cm^{-1}, and 1596 cm^{-1}, 1585 cm^{-1} remained unaffected during the change of buffer, suggesting that they are not due to the interactions between inorganic phosphate and IAP. The intensities of the negative peaks located around 1631 cm^{-1} and 1639 cm^{-1} decreased in intensity when the Tris-HCl buffer was changed for the phosphate buffer.

Second, control samples containing 5 mM adenosine were used to saturate the eventual adenosine-binding site of IAP. The RIDS of 5 mM NPE-caged ATP with IAP but without adenosine in Tris-HCl buffer p^2H 7.0 (Fig. 8 *A*) was almost identical to that of NPE-caged ATP with IAP and 5 mM adenosine in the same buffer (Fig. 8 *C*). Similar RIDS of IAP in phosphate buffer without (Fig. 8 *B*) or with adenosine (Fig. 8 *D*) were obtained. Taken together, the results presented in Fig. 8 suggest that adenosine did not interact with IAP.

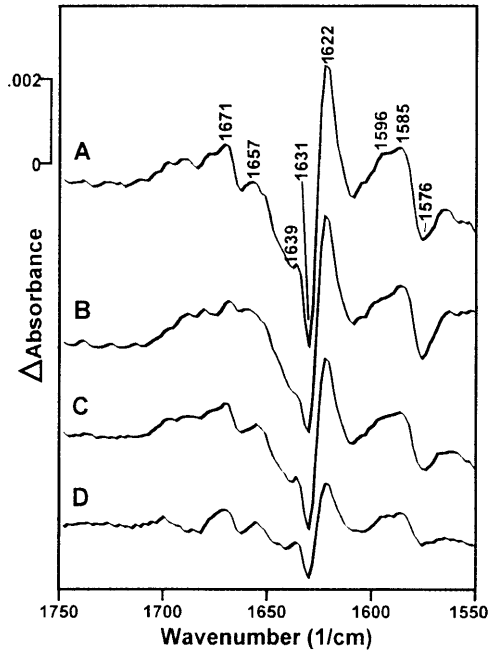

FIGURE 7 Reaction-induced infrared difference spectra of intestinal alkaline phosphatase produced by the photorelease of ATP. Effects of the increase of the NPE-caged ATP concentration on the structure of IAP. Trace *A* is the RIDS of 10 mM caged ATP with IAP. Trace *B* is the RIDS of 7.5 mM caged ATP with IAP. Trace *C* is the RIDS of 5 mM caged ATP with IAP. Trace *D* is the RIDS of 2.5 mM caged ATP with IAP. All the RIDS were corrected for the contribution of photolysis of NPE-caged ATP in the infrared spectra (see Fig. 2). Buffer composition was 100 mM Tris-HCl, $p^2H = 7.0$, 10 mM $MgCl_2$, and 10 mg/ml (0.09 mM) IAP with the indicated concentrations of NPE-caged ATP.

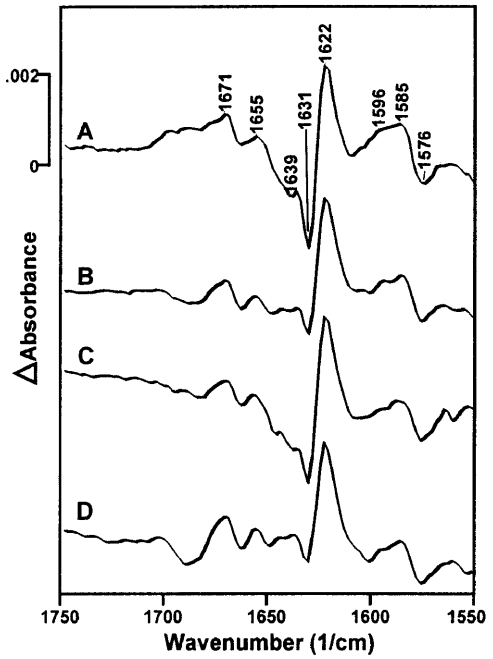

FIGURE 8 Reaction-induced infrared difference spectra of intestinal alkaline phosphatase produced by the photorelease of ATP. Effects of *Pi* and adenosine on the structure of IAP. Trace *A* is the RIDS of IAP without adenosine in Tris-HCl buffer (5 mM caged ATP with 10 mg/ml (0.09 mM) IAP in buffer containing 100 mM Tris-HCl, $p^2H = 7.0$, and 10 mM $MgCl_2$). Trace *B* is the RIDS of IAP in phosphate buffer (5 mM caged ATP with 10 mg/ml (0.09 mM) IAP in buffer containing 100 mM phosphate, $p^2H = 7.0$, 10 mM $MgCl_2$). Trace *C* is the RIDS of IAP in the presence of adenosine (5 mM caged ATP with 10 mg/ml (0.09 mM) IAP and 5 mM adenosine in buffer containing 100 mM Tris-HCl, $p^2H = 7.0$, 10 mM $MgCl_2$). Trace *D* is the RIDS of IAP in the presence of adenosine and phosphate (5 mM caged ATP with 10 mg/ml IAP and 5 mM adenosine in buffer containing 100 mM phosphate, $p^2H = 7.0$, 10 mM $MgCl_2$).

Thirdly, RIDS of 0.09 mM IAP in Tris-HCl buffer p^2H 7.0 containing 5 mM NPE-caged ATP, 10 mM Mg^{2+}, and 50 mM L-Phe (an uncompetitive inhibitor of IAP as well as a derivative of 2-nitrosoacetophenone) was identical to the RIDS of IAP under the same conditions but without L-Phe (results not shown). This indicates that the uncompetitive site of IAP was not involved in the structural changes. The infrared changes observed at 1631 cm^{-1} and 1639 cm^{-1} could indicate interactions between phosphate groups with IAP although other interpretations cannot be excluded. The peaks located at 1670–1671 cm^{-1}, 1651–1658 cm^{-1}, and 1596 cm^{-1} may signal interactions between IAP with 2-nitrosoacetophenone.

DISCUSSION

Light-induced infrared difference spectroscopy

The basic idea of difference infrared spectroscopy is to get rid of the enormous background absorbance from the many groups of the protein not involved in the ligand binding. Any absorbance related to protein moiety and to buffer which do not participate in the ligand binding is canceled in the difference infrared spectrum. Although one can obtain a difference spectrum by comparing the infrared spectra of different samples, the experimental errors due to protein or buffer concentrations are often larger than the expected differences caused by ligand binding. Therefore, photolytic release of substrate from inactive caged-substrate enables investigation of molecule-protein reaction directly in the cuvette, thereby minimizing experimental errors due to protein and buffer concentrations (Mäntele, 1993; Siebert, 1995; Cepus et al., 1998; Zscherp and Barth, 2001; Barth and Zscherp, 2002). NPE-caged ATP was selected as alkaline phosphatase substrate since it is commercially available and it is conveniently used to monitor structural changes caused by nucleotide binding (Troullier et al., 1996; Raimbault et al., 1997; Von Germar et al., 1999; Geibel et al., 2000; Allin and Gerwert, 2001; Granjon et al., 2001; Butler et al., 2002; Kirilenko et al., 2002; Liu and Barth, 2003).

Structural changes related to phosphate-binding induced changes in the active site

The overall infrared changes that were observed in the amide-I region, after photorelease and complete hydrolysis

of 5 mM ATP by mammalian IAP in aqueous solution, corresponded to the involvement of 2 amino acid residues per monomer IAP, based on the ratio of infrared intensities as determined by COBSI index. This index is a measure of change of backbone structure and interactions and may underestimate the number of amino acid residues affected, due to band overlapping (Barth et al., 1996; Scheirlinckx et al., 2001). We cannot neglect the phosphodiesterase activity of IAP, before the photorelease of ATP from the NPE-caged ATP, especially when the IAP concentration was high (0.45 mM dimeric IAP in H_2O Tris-HCl buffer), contributing to underestimation of the number of amino acid residues affected. The phosphodiesterase activity, although very small (it is about 10^6 times lower than the monophosphoesterase activity) was clearly assigned to *E. coli* alkaline phosphatase and not to any phosphodiesterase contaminant (O'Brien and Herschlag, 2002). Therefore, to better observe the structural changes caused by the phosphate binding, it was necessary to decrease IAP concentration (down to 0.09 mM) and to increase the NPE-caged ATP (from 2mM to 10 mM). The comparison of the RIDS of IAP in 100 mM Tris-HCl buffer pH 7.4, favoring the formation of a Tris-phosphate complex and its dissociation (k_5 and k_6, Scheme 1) (Trentham and Gutfreund, 1968) or in 100 mM phosphate buffer (saturating the active site with P*i*) allowed us to identify putative infrared changes associated with phosphate groups. These changes consisted in a decrease in intensities of the infrared bands located at 1631 cm^{-1} and at 1639 cm^{-1}, suggesting a very small distortion of the peptide carbonyl backbone. Based on the relative ratio of infrared intensities, these changes corresponded to less than one amino acid residue. Whether the changes in the intensities of the two bands are solely related to the interactions of phosphate groups with IAP remains to be further investigated. Nevertheless, these results indicate that the difference between IAP and IAP-P*i* complex in water medium involved only very small structural changes. Recently, x-ray diffraction data indicated that VO_4^{3-} was bound in the active site of *E. coli* AP, providing a structural model for the transition state in the enzyme catalyzed reaction (Holtz et al., 1999). Comparison between *E. coli* AP-vanadate complex and *E. coli* AP-P*i* complex shows that the active site residues move only slightly to accommodate the transition state (Holtz et al., 1999). Our work indicates that P*i* binding induced only minimal structural changes for the mammalian IAP, in accordance with the x-ray results on *E. coli* AP. In addition, RIDS did not reveal that water molecules could affect the conformational changes induced by P*i*-binding. Although water molecules may surround the charged P*i* groups, it appears that the binding of P*i* to IAP in aqueous medium had no additional structural effects on IAP. This tends to suggest that P*i* or vanadate binding involve only elastic collisions and is consistent with alkaline phosphatase being a ''perfect enzyme'' at pH range from 7 to 8 (Simopoulos and Jencks, 1994; O'Brien and Herschlag, 2001,2002), where k_{cat}/K_m (as determined for the *E. coli* enzyme) is maximum. The mechanism of P*i* inhibition is probably not associated with conformational changes but P*i* may serve passively to hinder the active site.

Structural changes due to the interaction of 2-nitrosoacetophenone with alkaline phosphatase

The photolysis of NPE-caged ATP produced 2-nitrosoacetophenone (free cage) and ATP, which was sequentially hydrolyzed by IAP giving rise to adenosine and three P*i*. Since only a part of the RIDS could be assigned to the conformational changes induced by the interactions of P*i* with IAP, the remaining part could be related to the interactions of adenosine, 2-nitrosoacetophenone or NPE-caged ATP with IAP. Indeed, saturation of P*i*, interacting with the active site, did not completely hinder the infrared changes, thus indicating that P*i* binding could not have induced all the infrared changes. Addition of 5 mM of adenosine did not prevent the infrared changes, suggesting that adenosine did not interact with IAP. Therefore, it was concluded that NPE-caged ATP or 2-nitrosoacetophenone could induce structural changes at 1670–1671 cm^{-1}, 1651–1658 cm^{-1}, and 1596 cm^{-1}, affecting at least one or two amino acid residues of the peptide backbone when considering the ratio of infrared intensities in the amide-I region. The location of the binding site of 2-nitrosoacetophenone with IAP is outside of the active site of IAP and the uncompetitive binding site of L-Phe in IAP, since the addition of 100 mM phosphate or 50 mM L-Phe in IAP samples could not prevent completely the infrared changes of the protein in the amide-I region.

REFERENCES

Allin, C., and K. Gerwert. 2001. Ras catalyzes GTP hydrolysis by shifting negative charges from gamma- to beta- phosphate as revealed by time-resolved FTIR difference spectroscopy. *Biochemistry*. 40:3037–3046.

Barth, A. 2000. The infrared absorption of amino acid side chains. *Prog. Biophys. Mol. Biol.* 74:141–173.

Barth, A., J. T. E. Corie, M. J. Gradwell, Y. Maeda, W. Mäntele, T. Meier, and D. R. Trentham. 1997. Time-resolved infrared spectroscopy of intermediates and products from photolysis of 1-(2-Nitrophenyl)ethyl phosphates: Reaction of the 2-Nitrosoacetophenone byproducts with thiols. *J. Am. Chem. Soc.* 119:4149–4159.

Barth, A., W. Kreutz, and W. Mäntele. 1990. Molecular changes in the sarcoplasmic reticulum calcium ATPase during catalytic activity. A Fourier transform infrared (FTIR) study using photolysis of caged ATP to trigger the reaction cycle. *FEBS Lett.* 277:147–150.

Barth, A., W. Mäntele, and W. Kreutz. 1991. Infrared spectroscopic signals arising from ligand binding and conformational changes in the catalytic cycle of sarcoplasmic reticulum calcium ATPase. *Biochim. Biophys. Acta.* 1057:115–123.

Barth, A., F. Von Germar, W. Kreutz, and W. Mäntele. 1996. Time-resolved infrared spectroscopy of the Ca^{2+}-ATPase. The enzyme at work. *J. Biol. Chem.* 271:30637–30646.

Barth, A., and C. Zscherp. 2002. What vibrations tell us about proteins. *Q. Rev. Biophys.* 35:369–430.

Butler, B. C., R. H. Hanchett, H. Rafailov, and G. MacDonald. 2002. Investigating structural changes induced by nucleotide binding to RecA using difference FTIR. *Biophys. J.* 82:2198–2210.

Berger, J., E. Garattini, J.-C. Hua, and S. Udenfriend. 1987. Cloning and sequencing of human intestinal alkaline phosphatase cDNA. *Proc. Natl. Acad. Sci. USA.* 84:695–698.

Bortolato, M., Besson, F., and Roux, B. 1999. An infrared study of the thermal and pH stabilities of the GPI-alkaline phosphatase from bovine intestine. *Proteins.* 37: 310–318.

Bradshaw, R. A., F. Cancedda, L. H. Ericsson, P. A. Newman, S. P. Piccoli, M. J. Schlessinger, K. Shriefer, and K. A. Walsh. 1981. Amino acid sequence of *Escherichia coli* alkaline phosphatase. *Proc. Natl. Acad. Sci. USA.* 78:3473–3477.

Butler, B. C., R. H. Hanchett, H. Rafailov, and G. MacDonald. 2002. Investigating structural changes induced by nucleotide binding to RecA using difference FTIR. *Biophys. J.* 82:2198–2210.

Byers, D. A., H. N. Fernley, and P. G. Walker. 1972. Studies on alkaline phosphatase. Inhibition of human-placental phosphoryl phosphatase by L-phenylalanine. *Eur. J. Biochem.* 29:197–204.

Cepus, V., C. Ulbrich, C. Allin, A. Trouiller, and K. Gerwert. 1998. Fourier transform infrared photolysis studies of caged compounds. *Methods Enzymol.* 291:223–245.

Chang, C. N., W.-J. Kuang, and E. Y. Cheng. 1986. Nucleotide sequence of the alkaline phosphatase gene of Escherichia coli. *Gene.* 44:121–125.

Chirgadze, Y. N., O. V. Fedorov, and N. P. Trushina. 1975. Estimation of amino acid residue side-chain absorption in the infrared spectra of protein solutions in heavy water. *Biopolymers.* 14:679–694.

Chlebowski, J. F., I. M. Armitage, and J. E. Coleman. 1977. Allosteric interactions between metal ion and phosphate at the active sites of alkaline phosphatase as determined by 31P NMR and 113Cd NMR. *J. Biol. Chem.* 252:7053–7061.

Chlebowski, J. F., and J. E. Coleman. 1972. Presteady state kinetics of phosphorothioate hydrolysis by alkaline phosphatase. *J. Biol. Chem.* 247:6007–6010.

de La Fournière, L., O. Nosjean, R. Buchet, and B. Roux. 1995. Thermal and pH stabilities of alkaline phosphatase from bovine intestinal mucosa: a FTIR study. *Biochim. Biophys. Acta.* 1248:186–192.

Fernley, H. N. 1971. Mammalian alkaline phosphatase. *In* The Enzymes, 3rd ed. P. D. Boyer, editor. Academic Press, New York and London. 417–447.

Ferguson, M. A. J. 1999. The structure, biosynthesis and functions of glycosyl-phosphatidylinositol anchors, and the contributions of trypanosome research. *J. Cell Sci.* 112:2799–2809.

Fishman, W., and H. G. Sie. 1970. L-homoarginine; an inhibitor of serum ''bone and liver'' alkaline phosphatase. *Clin. Chim. Acta.* 29:339–341.

Fishman, W. H., and H. G. Sie. 1971. Organ-specific inhibition of human alkaline phosphatase isoenzymes of liver, bone, intestine and placenta; L-phenylalanine, L-tryptophan and L-homoarginine. *Enzymologia.* 41: 141–167.

Geibel, S., A. Barth, S. Amslinger, A. H. Jung, C. Burzik, R. J. Clarke, R. S. Givens, and K. Fendler. 2000. P(3)-[2-(4-hydroxyphenyl)-2-oxo]ethyl ATP for the rapid activation of the Na(+), K(+)-ATPase. *Biophys. J.* 79:1346–1357.

Gettins, P., and J. E. Coleman. 1983. ^{31}P nuclear magnetic resonance of phospho-enzyme intermediates of alkaline phosphatase. *J. Biol. Chem.* 258:408–416.

Glasoe, P. K., and F. A. Long. 1960. Use of glass electrodes to measure acidities in deuterium oxide. *J. Phys. Chem.* 64:188–190.

Goormaghtigh, E., V. Cabiaux, and J.-M. Ruysschaert. 1994a. Subtraction of atmospheric water contribution in Fourier transform infrared spectroscopy of biological membranes and proteins. *Spectrochim. Acta, Part A.* 51A:2137–2144.

Goormaghtigh, E., V. Cabiaux, and J.-M. Ruysschaert. 1994b. Determination of soluble and membrane protein structure by Fourier transform infrared spectroscopy. II. Experimental aspects, side chain structure, and H/D exchange. *Subcell. Biochem.* 23:363–403.

Granjon, T., M.-J. Vacheron, C. Vial, and R. Buchet. 2001. Structural changes of mitochondrial creatine kinase upon binding of ADP, ATP, or P*i*, observed by reaction-induced infrared difference spectra. *Biochemistry.* 40:2988–2994.

Henthorn, P. S., M. Raducha, Y. H. Edwards, M. J. Weiss, C. Slaughter, M. A. Lafferty, and H. Harris. 1987. Nucleotide and amino acid sequences of human intestinal alkaline phosphatase: close homology to placental alkaline phosphatase. *Proc. Natl. Acad. Sci. USA.* 84:1234–1238.

Henthorn, P. S., M. Raducha, T. Kadesch, M. J. Weiss, and H. Harris. 1988. Structure of the human liver/bone/kidney alkaline phosphatase gene. *J. Biol. Chem.* 263:12011–12019.

Holtz, K. M., and E. R. Kantrowitz. 1999. The mechanism of the alkaline phosphatase reaction: insights from NMR, crystallography and site-specific mutagenesis. *FEBS Lett.* 462:7–11.

Holtz, K. M., B. Stec, and E. R. Kantrowitz. 1999. A model of the transition state in the alkaline phosphatase reaction. *J. Biol. Chem.* 274:8351–8354.

Hoylaerts, M. F., T. Manes, and J. L. Millán. 1992. Molecular mechanism of uncompetitive inhibition of human placental and germ-cell alkaline phosphatase. *Biochem. J.* 286:23–30.

Hoylaerts, M. F., T. Manes, and J. L. Millán. 1997. Mammalian alkaline phosphatases are allosteric enzymes. *J. Biol. Chem.* 272:22781–22787.

Hull, W. E., S. E. Halford, H. Gutfreund, and B. D. Sykes. 1976. ^{31}P nuclear magnetic resonance study of alkaline phosphatase: The role of inorganic phosphate in limiting the enzyme turnover rate at alkaline pH. *Biochemistry.* 15:1547–1561.

Hummer, G., and J. L. Millán. 1991. Gly429 is the major determinant of uncompetitive inhibition of human germ cell alkaline phosphatase by L-leucine. *Biochem. J.* 274:91–95.

Kam, W., E. Clauser, Y. S. Kim, Y. W. Kan, and W. Rutter. 1985. Cloning, sequencing, and chromosomal localization of human term placental alkaline phosphatase cDNA. *Proc. Natl. Acad. Sci. USA.* 82:8715–8719.

Kim, E. E., and H. W. Wyckoff. 1990. Structure of alkaline phosphatases. *Clin. Chim. Acta.* 186:175–188.

Kim, E. E., and H. W. Wyckoff. 1991. Reaction mechanism of alkaline phosphatase based on crystal structures. Two-metal ion catalysis. *J. Mol. Biol.* 218:449–464.

Kirilenko, A., M. Golczak, S. Pikula, R. Buchet, and J. Bandorowicz-Pikula. 2002. GTP-induced membrane binding and ion channel activity of annexin VI: is annexin VI a GTP biosensor? *Biophys. J.* 82:2737–2745.

Kozlenkov, A., T. Manes, M. F. Hoylaerts, and J. L. Millan. 2002. Function assignment to conserved residues in mammalian alkaline phosphatases. *J. Biol. Chem.* 277:22992–22999.

Le Du, M.-H., and J.-L. Millán. 2002. Structural evidence of functional divergence in human alkaline phosphatases. *J. Biol. Chem.* 277:49808–49814.

Le Du, M.-H., T. Stigbrand, M. J. Tausig, A. Ménez, and E. A. Stura. 2001. Crystal structure of alkaline phosphatase from human placenta at 1.8 Å resolution. Implication for a substrate specificity. *J. Biol. Chem.* 276: 9158–9165.

Lin, C. W., H. G. Sie, and W. H. Fishman. 1971. L-tryptophan. A non-allosteric organ-specific uncompetitive inhibitor of human placental alkaline phosphatase. *Biochem. J.* 124:509–516.

Liu, M., and A. Barth. 2003. Mapping interactions between the Ca^{2+} ATPase and its substrate ATP with infrared spectroscopy. *J. Biol. Chem.* 278:10112–10118.

Low, M. G., and J. B. Finean. 1977. Release of alkaline phosphatase from membranes by a phosphatidylinositol-specific phospholipase C. *Biochem. J.* 167:281–284.

Manes, T., M. F. Hoylaerts, R. Müller, F. Lottspeich, W. Hölke, and J. L. Millán. 1998. Genetic complexity, structure, and characterization of highly active bovine intestinal alkaline phosphatases. *J. Biol. Chem.* 273:23353–23360.

Mäntele, W. 1993. Reaction-induced infrared difference spectroscopy for the study of protein function and reaction mechanisms. *Trends Biochem. Sci.* 18:197–202.

Millán, J.-L. 1986. Molecular cloning and sequence analysis of human placental alkaline phosphatase. *J. Biol. Chem.* 261:3112–3115.

Millán, J.-L. 1988. Oncodevelopmental expression and structure of alkaline phosphatase genes. *Anticancer Res.* 8:995–1004.

Millán, J.-L., and T. Manes. 1988. Seminoma-derived Nagao isozyme is encoded by a germ-cell alkaline phosphatase gene. *Proc. Natl. Acad. Sci. USA.* 85:3024–3028.

Moss, D. W. 1992. Perspectives in alkaline phosphatase research. *Clin. Chem.* 38:2486–2492.

O'Brien, P. J., and D. Herschlag. 2001. Functional interrelationships in the alkaline phosphatase superfamily: phosphodiesterase activity of *Escherichia coli* alkaline phosphatases. *Biochemistry.* 40:5691–5699.

O'Brien, P. J., and D. Herschlag. 2002. Alkaline phosphatase revisited: hydrolysis of alkyl phosphates. *Biochemistry.* 41:3207–3225.

Raimbault, C., F. Besson, and R. Buchet. 1997. Conformational changes of arginine kinase induced by photochemical release of nucleotides from caged nucleotides: an infrared difference-spectroscopy investigation. *Eur. J. Biochem.* 244:343–351.

Redman, C. A., J. E. Thomas-Oates, S. Ogata, Y. Ikehara, and M. A. Ferguson. 1994. Structure of the glycosylphosphatidylinositol membrane anchor of human placental alkaline phosphatase. *Biochem. J.* 302:861–865.

Reid, T. W., and I. B. Wilson. 1971. *E. coli* alkaline phosphatase. *In* The Enzymes, 3rd ed. P. D. Boyer, editor. Academic Press, New York and London. 373–415.

Sarrouilhe, D., P. Lalegerie, and M. Baudry. 1993. Alkaline phosphatase activity at physiological pH: kinetic properties and biological significance. *Cell. Mol. Biol.* 39:13–19.

Scheirlinckx, F., R. Buchet, J.-M. Ruysschaert, and E. Goormaghtigh. 2001. Monitoring of secondary and tertiary structure changes in the gastric H^+/K^+-ATPase by infrared spectroscopy. *Eur. J. Biochem.* 268:3644–3653.

Siebert, F. 1995. Infrared spectroscopy applied to biochemical and biological problems. *Methods Enzymol.* 246:501–526.

Simopoulos, T. T., and W. P. Jencks. 1994. Alkaline phosphatase is an almost perfect enzyme. *Biochemistry.* 33:10375–10380.

Trentham, D. R., and H. Gutfreund. 1968. The kinetics of the reaction of nitrophenyl phosphates with alkaline phosphatase from *Escherichia coli*. *Biochem. J.* 106:455–460.

Troullier, A., K. Gerwert, and Y. Dupont. 1996. A time-resolved Fourier transformed infrared difference spectroscopy study of the sarcoplasmic reticulum Ca(2+)-ATPase: kinetics of the high-affinity calcium binding at low temperature. *Biophys. J.* 71:2970–2983.

Venyaminov, S. Y., and N. N. Kalnin. 1990. Quantitative IR spectrophotometry of peptide compounds in water (H_2O) solutions. I. Spectral parameters of amino acid residue absorption bands. *Biopolymers.* 30:1243–1257.

Von Germar, F., A. Galan, O. Llorca, J. L. Carrascoa, J. M. Valpuesta, W. Mäntele, and A. Muga. 1999. Conformational changes generated in GroEL during ATP hydrolysis as seen by time-resolved infrared spectroscopy. *J. Biol. Chem.* 274:5508–5513.

Weiss, M. J., P. S. Henthorn, M. A. Lafferty, C. Slaughter, M. Raducha, and H. Harris. 1986. Nucleotide and amino acid sequences of human intestinal alkaline phosphatase: close homology to placental alkaline phosphatase. *Proc. Natl. Acad. Sci. USA.* 83:7182–7186.

Weissig, H., A. Schildge, M. F. Hoylaerts, M. Iqbal, and J. L. Millán. 1993. Cloning and expression of the bovine intestinal alkaline phosphatase gene: biochemical characterization of the recombinant enzyme. *Biochem. J.* 290:503–508.

Zscherp, C., and A. Barth. 2001. Reaction-induced infrared difference spectroscopy for the study of protein reaction mechanisms. *Biochemistry.* 40:1875–1883.